ISSN 1995-0780, Nanotechnologies in Russia, 2014, Vol. 9, Nos. 11–12, pp. 723–727. © Pleiades Publishing, Ltd., 2014.
Original Russian Text © E.V. Sukovatitsina, A.S. Samardak, A.V. Ognev, L.A. Chebotkevich, M.R. Sanaeian, F. Nasirpouri, 2014, published in Rossiiskie Nanotekhnologii, 2014, Vol. 9, Nos. 11–12.

Dependence of the Magnetic Properties of Nanocrystalline Nickel Films on Grain Size and Surface Morphology

E. V. Sukovatitsina[a], A. S. Samardak[a, b], A. V. Ognev[a, b], L. A. Chebotkevich[a, b], M. R. Sanaeian[c], and F. Nasirpouri[c]

[a] *Far Eastern Federal University, ul. Sukhanova 8, Vladivostok, 690950 Russia*
[b] *Institute of Automatics and Control Processes, ul. Radio 5, Vladivostok, 690950 Russia*
[c] *Faculty of Materials Engineering, Sahand University of Technology, Tabriz, Iran*
e-mail: sukovatitsinaev@gmail.com; samardak.as@dvfu.ru

Received March 24, 2014; in final form, August 14, 2014

Abstract—Nickel films prepared by direct-current, pulse-current, and pulse reverse-current electrodeposition are studied. Scanning electron microscopy and atomic force microscopy show that the films consist of fine grains. The electrodeposition conditions are varied to prepare films with different grain sizes and surface roughness. All the films are magnetically isotropic. In films with a grain size comparable to the width of Bloch domain walls, the magnetization reversal occurs owing to the incoherent rotation of magnetization. In films with a grain size of more than 350 nm, the magnetization reversal occurs not only through the incoherent rotation of magnetization, but also owing to the nucleation and displacement of the domain walls.

DOI: 10.1134/S1995078014060160

INTRODUCTION

Nanocrystalline films [1, 2] with a grain size of less than 100 nm are used in industry owing to their improved physical, chemical, and mechanical properties [3, 4]. For example, nanocrystalline nickel films attract considerable attention because they exhibit high hardness, corrosion resistance, and wear resistance and have unique functional characteristics [5–8]. Electrodeposition is one of the most commonly used, simplest, and most adaptable methods for the production of thin metal films, such as nickel films [9]. There are a few electrodeposition methods: direct-current (DC), pulse-current (PC), and pulse reverse-current (PRC) electrodeposition. These three methods have different effects on the electrodeposition mechanism and the morphology of the resulting films, as will be shown in this study for nickel films.

DC electrodeposition has a number of disadvantages, such as a slow deposition rate of materials and a high imperfection of the films (surface roughnesses, high porosity, poor adhesion, and undesirable microstructure). The application of an alternating current makes it possible to overcome these difficulties owing to the periodic change in the concentration of ions of the deposited material at the interface, the magnitude of which decreases with increasing current frequency [10]. Therefore, PC and PRC electrodeposition methods have been developed in order to increase the deposition rate of materials and improve the film microstructure to achieve the desired functional properties [11–15]. The current alternates between a positive value and zero during PC deposition and between a positive and negative value in the event of PRC. The application of a zero current and a reverse current in the case of PC and PRC, respectively, effectively discharges the electric double layer formed around the cathode; this leads to a much better penetration of the ions of the deposited material in the direction of the cathode. Owing to this, the deposition rate increases. In addition, pulse techniques improve the uniformity of the distribution of the ions in the electrolyte and increase the area and quality of coating of the deposited films [16, 17].

In this study, Ni films prepared by DC, PC, and PRC electrodeposition are examined. Detailed examinations of the effect of deposition conditions on the evolution of the microstructure and the magnetic properties of the nickel films are described.

EXPERIMENTAL

Nickel films were prepared by electrodeposition in a Watts bath. A nickel plate (an area of 10 cm^2) with a purity of 99.99% was used as the anode. A copper foil (an area of 1 cm^2) was employed as the cathode. Electrodeposition was conducted from solutions of $NiSO_4 \cdot 6\,H_2O$ (265 g/L H_2O), $NiCl_2 \cdot 6\,H_2O$ (48 g/L H_2O), and H_3BO_3 (31 g/L H_2O). The acidity pH of the solution was 3.7. The temperature was maintained at 45 ± 0.5°C. Nanocrystalline nickel films were prepared applying a DC, PC, and PRC. In the case of the pulse method, the current alternated between a positive value and zero. In the event of a PRC, the current alternated between a positive and negative value. The

Parameters of electrodeposition of nanocrystalline nickel films

Electrodeposition conditions	
DC deposition	
Current density	100 mA/cm^2
Electrolyte stirring (magnetic stirrer)	400 rpm
PC deposition	
Peak current density	100 mA/cm^2
Electrolyte stirring (magnetic stirrer)	400 rpm
Pulse length	2 ms
Pause between pulses	18 ms
PRC deposition	
Peak current density of direct pulse	100 mA/cm^2
Peak current density of reverse pulse	100 mA/cm^2
Electrolyte stirring (magnetic stirrer)	400 rpm
Direct pulse length	2 ms
Pause after direct pulse	18 ms
Reverse pulse length	1 ms
Pause after reverse pulse	4 ms

current pulse had a rectangular shape. The electrodeposition conditions are shown in the table.

The pulse deposition technique provides a uniform distribution of the deposited material over the substrate surface, leading to an improvement of the microstructure and morphology of the films while maintaining the deposition rate of the metal.

Knowing current density I, deposition time t, molar mass M, and valence z of the ions, thickness D of the films was estimated from the Faraday formula $m = \rho D = It/F \times M/z$, where F is the Faraday constant. Since this method of determining the thickness is not accurate, all the arguments about magnetic properties will be related to the grain size, which was determined from images that were recorded using a high-resolution scanning electron microscope.

The structure and roughness of the films were studied by scanning electron microscopy (SEM) and atomic force microscopy (AFM), respectively. Coercive force and residual magnetization were determined from the magnetic hysteresis loops derived by the induction method using a highly sensitive vibromagnetometer in a magnetic field range of ±3000 Oe.

RESULTS AND DISCUSSION

The structure of nickel films of the same thickness that were prepared by DC, PC, and PRC methods was examined by SEM and is shown in Fig. 1. An analysis of the SEM images has shown that, in the films deposited by the DC method, the size and shape of the grains greatly differ (Fig. 1a). In the case of PC deposition, the crystallites have a polygonal shape and sharply defined faces, while the size range is significantly smaller than that of the films prepared by the DC method (Fig. 1b). PRC electrodeposition provides the formation of films with a smaller grain size and a lower porosity of the microstructure (Fig. 1c).

Using AFM, root-mean-square roughness amplitude h and mean roughness period L were determined for films of the same thickness prepared by the different methods. Thus, for the films with $D = 61.2$ μm prepared by the DC method, the average values are $h = 80$ nm and $L = 0.55$ μm; PC, $h = 50$ nm and $L = 0.60$ μm; and PRC, $h = 20$ nm and $L = 0.38$ μm. It is evident that the films prepared by the PRC method have the lowest roughness.

As a case in point, Fig. 2 shows AFM images of the films prepared by the PC method for different deposition times (with different thicknesses). The SEM images were used to determine the average grain size. As the film thickness increases, the grain size increases (Fig. 3). This, in turn, leads to an increase in film roughness (inset in Fig. 3).

In the studied polycrystalline films, induced anisotropy is absent, while the local crystallographic anisotropy leads to the isotropy of the magnetization reversal processes. This is confirmed by the polar diagrams of the reduced residual magnetization determined from the magnetic hysteresis loops (Fig. 4).

Figure 3 shows that the grain size of the Ni film with a thickness of 10.2 μm is on the order of 200 nm, which is comparable to the Bloch domain wall width of $\delta = \pi\sqrt{\frac{2A}{K_1}} = 190$ nm, where $A = 0.9 \times 10^{-6}$ erg/cm is the exchange interaction constant and $K_1 = 5 \times 10^4$ erg/cm^3 is the crystallographic anisotropy constant. Hence, the grains whose sizes are comparable to the domain wall width will be single-domain and, in each grain, the magnetization vector will be oriented along the crystallographic easy magnetization axis (EMA). Therefore, we can assume that, in films with grain sizes comparable to δ, the reversal magnetization processes occur owing to the incoherent rotation of the magnetization vector.

Films in which the grain size is significantly larger than the domain wall width can have a two-domain (multidomain) structure, which leads to a decrease in the magnetostatic energy of the grain. The magnetostatic energy of the grain can be estimated as $E_N = 0.5 H_N M_S = 0.5 N M_S^2 \approx 8 \times 10^5$ erg/cm^3, where N is the demagnetization factor of the grain. Therefore, in these films, the reversal magnetization processes occur owing to the displacement of the domain walls (which are located in the grain) and the incoherent rotation of magnetization. The occurrence of the

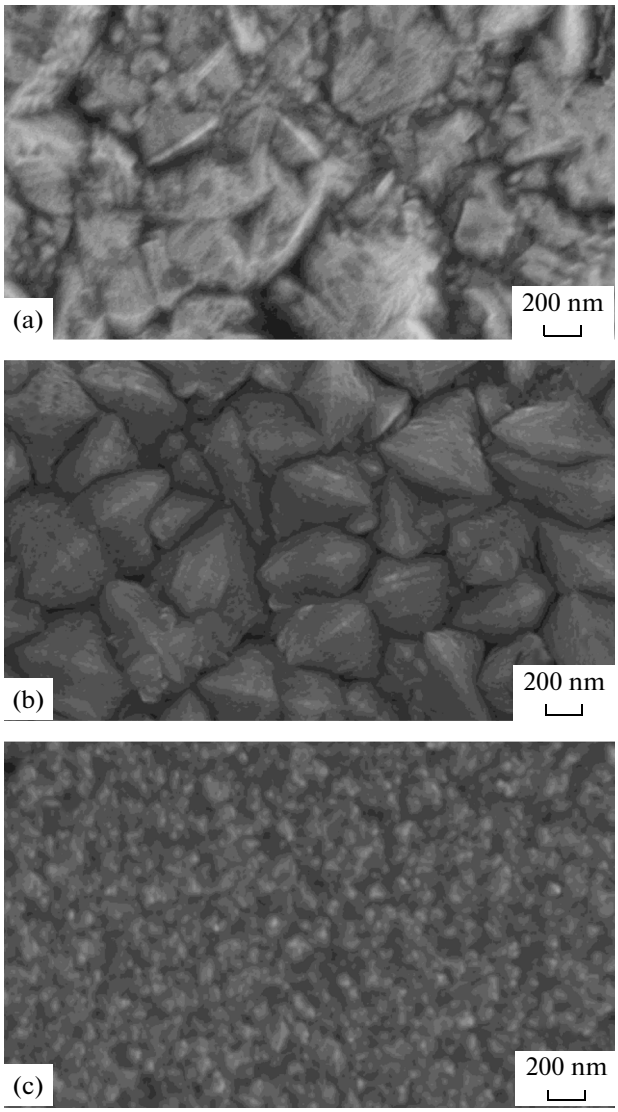

Fig. 1. SEM images of the Ni films prepared by (a) DC, (b) PC, and (c) PRC methods.

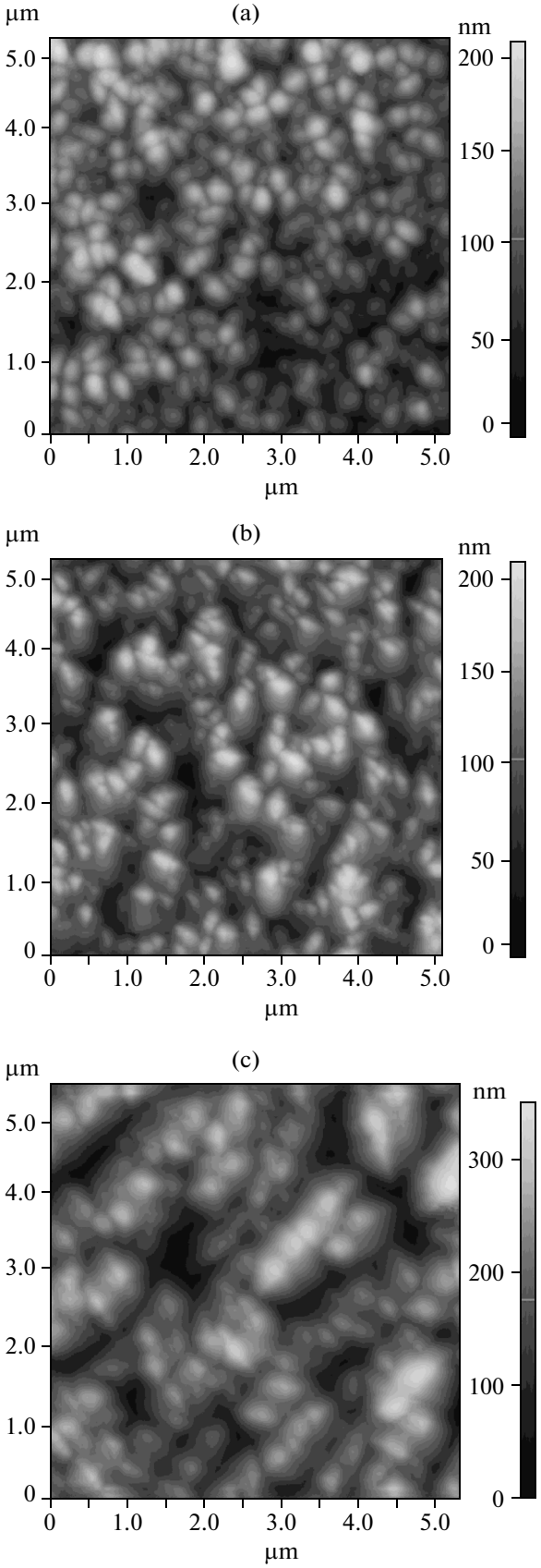

Fig. 2. AFM images of the surface of Ni films with thicknesses of (a) 10.2, (b) 20.4, and (c) 61.2 μm prepared by PC deposition.

incoherent rotation of the magnetization vector and the displacement of the domain walls in these films is proved by the magnetic hysteresis loops (inset in Fig. 5). These loops are extremely narrow and have the squareness ratio $M_r/M_s = 0.11–0.24$, where M_r is the residual magnetization and M_s is the saturation magnetization.

Experimental results have shown that coercive force H_c decreases with an increase in grain size. The dependence of H_c on R is shown in Fig. 5. It is known [18, 19] that the coercive force of polycrystalline films is determined by the pinning of the domain boundaries by structural defects. In polycrystalline films, these defects are grain boundaries, the disorientation of crystallographic EMAs, and surface roughnesses. According to the polar diagrams (Fig. 4), induced

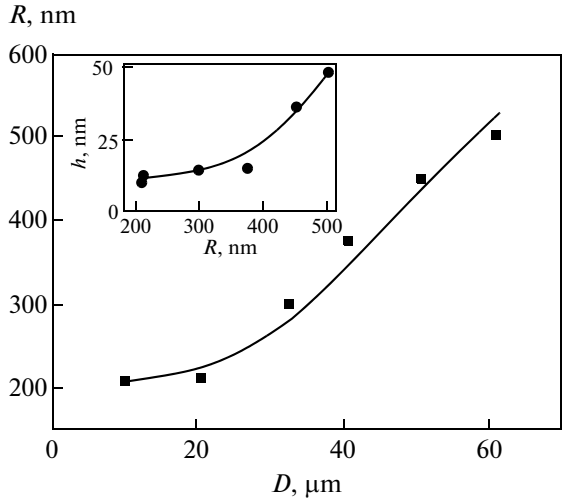

Fig. 3. Dependence of grain size R on thickness D of the film prepared by the PC method. The inset shows the dependence of roughness amplitude h on grain size R.

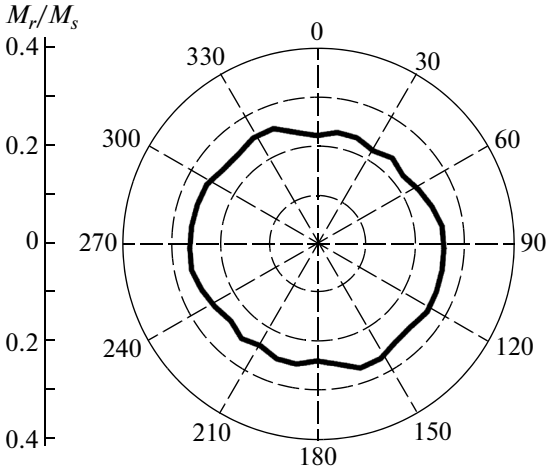

Fig. 4. Polar diagram of the squareness ratio M_r/M_s for film with a thickness of 10.2 μm.

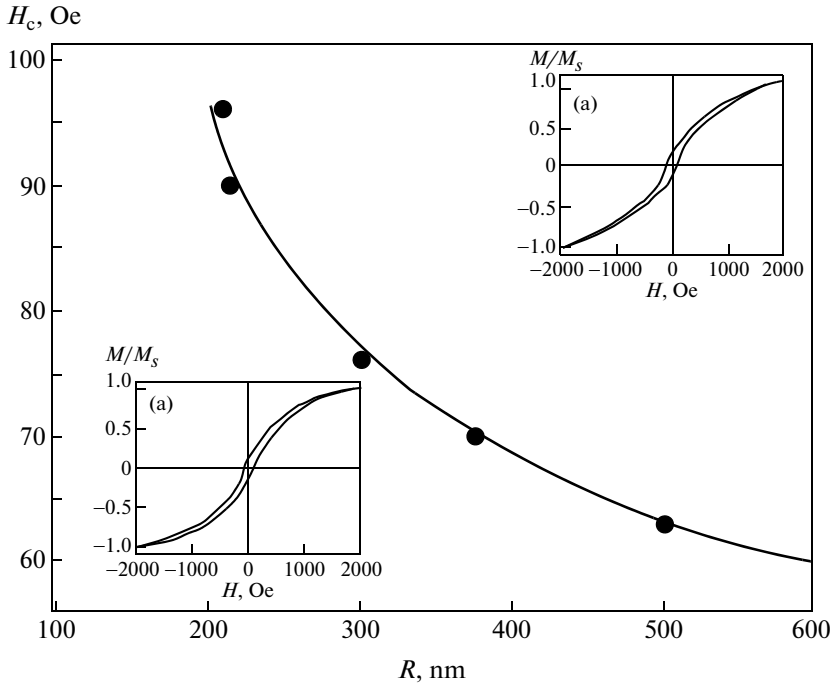

Fig. 5. Dependence of coercive force H_c on grain size R. The inset shows the hysteresis loops for films with thicknesses of (a) 10.2 and (b) 40.8 μm.

uniaxial anisotropy is absent in the studied films; consequently, there are no domain boundaries passing through a large number of grains. Therefore, in these films the above defects do not determine the coercive force magnitude. In single-domain grains, the magnetization vectors will be oriented along the crystallographic EMA of the grains. This effect is accompanied by the occurrence of magnetostatic fields of the grains [11]: $H_c^K = p_c \dfrac{K_1}{M_s}$, where $p_c = 0.64$ is the proportionality coefficient. Hence, $H_c^K = 63$ Oe. On the other hand, the film roughnesses generate a magnetostatic field [12]: $H_c^h = C\dfrac{M_s h \delta D^{1/3}}{(\delta + D)L^{4/3}}$, which also has an effect on the H_c value (here, C is the proportionality coefficient). Therefore, the coercive force of Ni films with single-domain grains can be represented as the sum of two components $H_c = H_c^K + H_c^h$ As the film

thickness increases, the $\frac{hD^{1/3}}{(\delta + D)L^{4/3}}$ ratio decreases. For example, for D = 10.2 μm, h = 10 nm, L = 200 nm, $H_c^h \approx 30$ Oe, and $H_c \approx 93$ Oe.

In polycrystalline Ni films with two-domain (multidomain) grains, H_c will be determined by the roughness and the pinning of the domain boundaries by the structural defects of the grain (dislocations) [13]: $H_c^{\text{disl}} = \frac{\langle F_{\max} \rangle}{2M_S S \cos\phi}$, where $\langle F_{\max} \rangle = l \times \sigma^m b$ is the maximum force of pinning of the domain boundary by dislocations, l is the total length of the dislocation line, b is the dislocation Burgers vector, σ^m is the domain boundary tension [14], $S = R\delta$ is the domain wall surface, and φ is the angle between the magnetization vector in the grain and the field. Dislocations in the grain can result from the mismatch of the lattice parameters of the film and the substrate (a_{Ni} = 0.35 nm, $a_{\text{Cu}} = 0.36$ nm). Even at a maximum dislocation density of 10^8 cm^{-2}, the number of dislocations in the grain cannot be more than one. Estimates give a value of $H_c^{\text{disl}} \approx 30$ Oe. For films with two-domain grains, the component $H_c^h \approx 18$ Oe; hence, $H_c \approx 48$ Oe. According to the estimates, upon switching from films with single-domain grains to films with two-domain grains, the coercive force decreases, which is consistent with the experimental data.

CONCLUSIONS

The study of the nanocrystalline nickel films prepared by electrodeposition has shown the following.

(1) The grain sizes and surface morphology of the films depend on the electrodeposition method. Films with the smallest grains (R < 100 nm) are formed by PRC deposition.

(2) In films with grain sizes comparable to the width of Bloch domain walls, the magnetization reversal processes occur owing only to the incoherent rotation of the magnetization vectors.

(3) In films with grain sizes significantly larger than the width of Bloch domain walls, the magnetization reversal processes occur owing to the nucleation and displacement of the domain boundaries and the incoherent rotation of the magnetization vectors.

(4) In films with single-domain grains (R < 350 nm), the H_c value is determined by the magnetostatic fields of the grains and the surface roughnesses, while in films with multidomain grains (R > 350 nm) it is determined by the pinning of the domain boundaries by dislocations and roughnesses.

ACKNOWLEDGMENTS

This work was supported by the Ministry of Education and Science of Russia, the Science Foundation of the Far Eastern Federal University, and OPTEK company.

REFERENCES

1. C. Suryanarayana and C. C. Koch, Hyperfine Interact. **130**, 5 (2000).
2. A. S. Samardak and L. A. Chebotkevich, Phys. Met. Metallogr. **101**, 11 (2006).
3. C. C. Koch and J. Sci. Mater. **42**, 1403 (2007).
4. R. Mishra, B. Basu, and R. Balasubramaniam, Mater. Sci. Eng. A **373**, 370 (2004).
5. A. Ul-Hamid, H. Dafalla, A. Quddus, H. Saricimen, and L. M. Al-Hadhrami, Appl. Surf. Sci. **257**, 9251 (2011).
6. A. V. Ognev, E. V. Sukovatitsina, L. A. Chebotkevich, K. S. Diga, S. M. Janjan, F. Nasirpouri, and A. S. Samardak, J. Phys.: Conf. Ser. **345**, 012010 (2012).
7. O. Sadiku-Agboola, E. R. Sadiku, O. I. Ojo, O. L. Akanji, and O. F. Biotidara, Portug. Electrochim. Acta **29**, 91 (2011).
8. F. Nasirpouri, A. Nogaret, D. Atkinson, M. Ghorbani, and A. Irajizad, J. Magn. Magn. Mater. **299**, 356 (2006).
9. F. Nasirpouri, S. M. Janjan, S. M. Peighambari, M. G. Hosseini, A. Akbari, and A. S. Samardak, J. Electroanal. Chem. **299**, 356 (2013).
10. H. Gerischer, Anal. Chem. **31**, 33–39 (1959).
11. T. Borkar and S. P. Harimkar, Surf. Coat. Tech. **205**, 4124–4134 (2011).
12. K. I. Popov, M. D. Maksimovic, and M. S. Simic, Surf. Technol. **16**, 209–218 (1982).
13. D. Landolt and A. Marlot, Surf. Coat. Technol., **169–170**, 8–13 (2003).
14. L. Shao, L. Du, and L. Wang, Micro Nano Lett. **5**, 165–170 (2010).
15. B. Tury, M. Lakatos-Varsányi, and S. Roy, Surf. Coat. Technol., **200**, 6713–6717 (2006).
16. N. V. Mandich, HBM Eng. Co. Lansing. **3**, 374–379.
17. L. M. Chang, J. Alloys Compounds, **466**, 19–22 (2008).
18. V. I. Malytin, V. E. Osukhovskii, A. A. Ivanov, L. A. Chebotkevich, I. V. Lobov, and Yu. D. Vorobitv, Phys. Status Solidi A **93**, 585–595 (1986).
19. A. A. Ivanov, Fiz. Met. Metalloved. **49**, 954 (1980).
20. G. Herzer, IEEE Trans. Magn. **26**, 1397 (1990).
21. S. P. Li, A. Samad, W. S. Lew, Y. B. Xu, and J. A. C. Bland, Phys. Rev. B. **61**, 6871 (2000).
22. R. Berner and H. Kronmüller, *Plastische Verformung von Einkristallen,* Ed. by A. Seeger (Springer-Verlag, Berlin, 1965).
23. G. Rieder, Abh. Brounshw. Wiss. Ges. **11**, 20 (1956).

Translated by M. Timoshinina